RSC Advances

ROYAL SOCIETY OF CHEMISTRY

www.rsc.org/advances

A facile method of synthesizing ammonia modified graphene oxide for efficient removal of uranyl ions from aqueous medium

Swati Verma, Raj Kumar Dutta*

Department of Chemistry, Indian Institute of Technology Roorkee, Roorkee 247667,

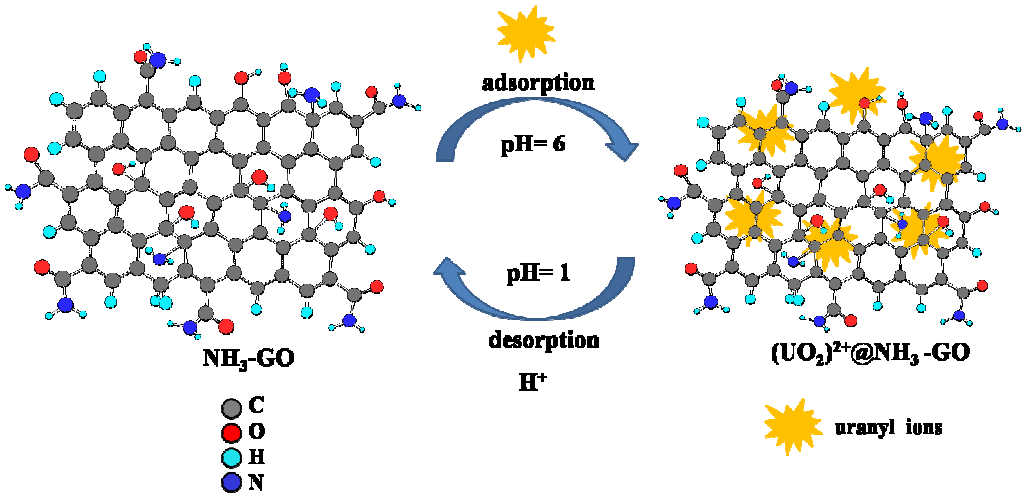

Adsorption of uranyl ions on NH_3 modified graphene oxide at pH 6

A facile method of synthesizing ammonia modified graphene oxide for an efficient removal of uranyl ions from aqueous medium

Swati Verma, Raj Kumar Dutta*

Department of Chemistry, Indian Institute of Technology Roorkee, Roorkee 247667,

Abstract

Graphene oxide has recently emerged as an efficient adsorbent for removal of heavy metals including radionuclides from contaminated ground water. Here we demonstrate very high adsorption capacity (q_e = 72.2 mg/g) of graphene oxide for adsorption of uranyl ions. But in the presence of common interfering cations (Ca^{2+}, Mg^{2+}, K^{+}, Na^{+}, Pb^{2+}, Fe^{2+} and Zn^{2+}) and anions (CO_3^{2-}, HCO_3^{-}, Cl^{-} and SO_4^{2-}) that are expected in ground water, the adsorption capacity of uranyl ions on graphene oxide decreased drastically owing to poor selectivity. Here we report a strategy for significantly improving selective adsorption of uranyl ions in the presence of the above interfering species. The graphene oxide is modified by liquid ammonia in presence of dehydrating agent (the material obtained is referred as NH_3-GO adsorbent) and thoroughly characterized by zeta potential measurement, Raman spectroscopy, Fourier transformed infrared spectroscopy, transmission electron microscopy and scanning electron microscopy. The suitability of NH_3-GO as an adsorbent of uranyl ions has been studied in batch mode as a function of pH, temperature, adsorbent dose and initial concentration of uranyl ions. The maximum experimental adsorption capacity at equilibrium condition is found 40.1 mg/g at pH 6 at 298 K, which is not affected due to the presence of the most of the cations and anions. This marked improvement in the selectivity of uranyl ion adsorption is attributed to amidation of graphene oxide, rendering improved selectivity as compared to carboxylic acid groups in

graphene oxide. The maximum monolayer coverage (q_{max}) was deduced as 80.13 mg/g, indicating an excellent adsorbent. The mechanism of adsorption is studied in terms of adsorption isotherm models, kinetic models and thermodynamic studies, which indicated dual mechanism of chemisorption and physisorption owing to more than one types of binding sites in NH_3-GO. It is concluded that the ammonia modified graphene oxide exhibited highly selective adsorption property of uranyl ions at neutral pH.

Keywords: Modified graphene oxide, Uranyl ions, Adsorption capacity, Chemisorption

* Corresponding Author: Email: duttafcy@iitr.ernet.in (R.K. Dutta), Tel. +91 1332 285280, Fax: +91 1332 286206

1. Introduction

Uranium is known to be hazardous to human system due to its radioactive property and toxicity effects.[1] Uranium is usually found in the environment in hexavalent form and its toxicity is reflected from carcinogenic and mutagenic characteristics.[2] The toxicity levels of uranium for human is reported even at trace levels, where World Health organization (WHO) and United States Environmental Protection Agency (USEPA) have regulated maximum concentration level of uranium in drinking water to be 0.015 and 0.030 mg/L, respectively.[3,4] The source of uranium in environmental domain may be broadly classified as anthropogenic and natural. The anthropogenic source is related to enhanced mining of uranium ores and their processing which is associated with increase in the volumes of effluents and therefore pose threat to environment. This necessitates suitable technology for removal of uranium and other radioactive toxicants

from the effluents of nuclear industries prior to their disposal into environment in order to minimize its adverse impact on human health.[5,6]

Several methods including nanotechnology have been developed for the removal of environmental contaminants.[7-11] The graphene based materials have emerged as an efficient and promising adsorbents heavy metal removals including those of radionuclides owing to favourable physicochemical properties e.g., high specific surface area and adsorption capacity, mechanical strength, radiation resistance and chemically stable in wide range of pH.[12,13] It may be remarked here that the graphene sheets comprising of hexagonal arrangement of sp^2 hybridized carbon atoms rendered hydrophobic property. Graphene based materials are reported to be excellent for various environmental application,[14,15] but their applications as an adsorbent for metal ion adsorption in aqueous medium is restricted due to hydrophobicity.[16] In this regard, modification of graphene to graphene oxide render hydrophilic property owing to the incorporation of carbonyl and carboxyl groups at the plane edges and hydroxyls and epoxides in the basal graphene plane.[17] Consequently, graphene oxide revealed excellent adsorption capacities for organic pollutants and heavy metals and uranyl ions.[18-20] However, the major drawback of GO as a sorbent is associated with the challenges for separating and recovering the sorbent after the adsorption process. This limitation has however been addressed by developing composites of graphene oxide and magnetite nanoparticles as adsorbent which could be magnetically separated.[21,22]

It is envisaged that graphene oxide comprising of carboxylic acid group might not be selective to only uranyl ions. Rather amines and amides are better ligands for binding with uranyl ions.[23-24] In view of this, amidation of carboxylic acid group is an option for functionalization of GO for uranyl ion adsorption. Various methods have been adopted for reduction of graphene oxide to

form amides, e.g., by treating with hydrazine, aniline, primary and secondary amines for selective metal ion adsorption including the uranyl ions.[25-29] In the present study, a simple method has been developed where graphene oxide nanosheets were reduced by liquid ammonia in dehydrating solvent for developing a suitable adsorbent that can be used for removal of uranyl ions at neutral pH or at mildly acidic pH. The purpose of choosing ammonia over hydrazine was to modify –COOH groups of graphene oxide into $–CONH_2$ groups to achieve higher specific binding with uranyl ions. Notably, graphene oxide reduced with hydarazine is reported to yield pyrazoles,[30] and the maximum adsorption capacity of uranium in this reduced graphene oxide was reported as 47.0 mg/g.[13] We have demonstrated the advantages of using ammonia modified graphene oxide for uranyl ion adsorption over graphene oxide as well as reduced graphene oxide as adsorbent. The quantitative determination of uranyl ions in this study is performed by colorimetric method by complexing uranyl species with arsenazo (III) dye. The adsorption study of uranyl ion on ammonia modified graphene oxide is optimized and the adsorption mechanism is studied in terms of adsorption kinetics and adsorption isotherm models.

2. *Materials and method*

2.1 Chemicals

Graphite powder (mesh size < 20 μm) and arsenazo (III) were procured from Sigma Aldrich, GmbH, Germany. Concentrated sulphuric acid (H_2SO_4, 98%) and ethylene glycol ($C_2H_4O_2$, 98%) and diethyl ether were purchased from Rankem, India Pvt. Ltd. Potassium permanganate ($KMnO_4$), liquid ammonia (NH_3, 30% v/v) and ortho-phosphoric acid (H_3PO_4, 88%) and uranyl nitrate hexahydrate, $UO_2(NO_3)_2.6H_2O$; M.W = 502 g) were purchased from Merck, India. All reagents used for the synthesis were of laboratory grade and were used without any further purification. De-ionised water (DI water, Millipore) has been used throughout this study.

2.2 Synthesis of ammonia modified graphene oxide

First graphene oxide (GO) was synthesized form graphite powder using Hummer's method with minor modifications.[31] Briefly, 60 mL of conc. H_2SO_4 and 6.67 mL H_3PO_4 were mixed and cooled in an ice bath. To this solution, 0.5 g of graphite powder and 3.0 g $KMnO_4$ was added. The reaction mixture was stirred for 12 h at 50 °C. This solution was cooled to room temperature and was treated with 1 mL of 30% H_2O_2 in ice water. The solid material formed at this stage was separated by centrifugation at 5000 rpm for 10 min. A shiny golden brown material was obtained which was washed sequentially with 30 mL DI water, 30 mL of 30% HCl, 30 mL of ethanol and finally coagulated using diethyl ether. The nanosheets of graphene oxide (GO) were exfoliated using ultra-sonication and were kept in Petri dish at room temperature for drying. 100 mg of the as-obtained GO was re-dispersed in 40 mL of ethylene glycol by ultra-sonication to form a brown coloured solution. A 100 µL of liq. ammonia was added to this solution which resulted in formation of a black colour solution, which was refluxed in a round bottom flask for 3 h at 180 °C using oil bath. After refluxing, the content was filtered in a Buchner funnel through Whatman filter paper No. 41. A black coloured solid material was obtained as a residue which was washed with DI water and left for oven drying at 50 °C. This material was referred to as NH_3 modified graphene oxide (NH_3-GO).

2.3 Characterization techniques

The morphology of the NH_3-GO was studied by transmission electron microscopy (TEM) operated at 200 kV FEI Technai - G² microscope and by field emission – Scanning Electron Microscope coupled with Energy Dispersive X-ray Analysis (FE-SEM, EDX, Zeiss ultraplus) operated at 15 kV. The samples for TEM studies were prepared by drop casting NH_3-GO nanosheets dispersed in de-ionized water on a carbon coated 150 mesh copper grid and dried at

room temperature. Similarly, the samples for FE-SEM studies were prepared by adhering NH_3-GO on a pre-cleaned glass plate and sputter coated with a thin layer of gold to impart conductivity for incident electrons. The XRD studies of GO and NH_3-GO were performed by powder X-ray diffractometer (Bruker ARS D8 advanced) using graphite monochromatized Cu K_α radiation source with a wavelength of 1.54 A° in a wide-angle region from 5° to 85° on 2θ scale with a scan rate of 2°/min operated at 40 kV. Raman spectra of GO and NH_3-GO were recorded using inVia Raman microscope (Renishaw) with an excitation energy of λ = 514 nm. The zeta potential of the as-synthesized GO and NH_3-GO nanosheets was measured at different pH after re-dispersing in DI water using Malvern Zetasizer Nano ZS90 instrument. The functional groups of GO and NH_3-GO were analyzed by recording FT-IR spectra using Nicolet, Nexus FT-IR spectrometer. Pellets of dried samples were made with KBr and were scanned in the range of 500 – 4000 cm^{-1}.

2.4 Batch adsorption studies

A stock solution of 1000 mg/L of uranium was prepared by dissolving 2.11 g of $UO_2(NO_3)_2.6H_2O$ in 1 L of DI water. Solutions of different concentrations of uranyl ions were prepared by diluting the uranium stock solution in de-ionized water. First the pH was optimized by performing adsorption studies at different pH of the uranyl ion solution ranging between 2 and 9. The other parameters like contact time (up to 4 h), adsorbent dose (10 mg – 70 mg), adsorbate concentration (5 mg/L to 100 mg/L) and effect of temperature (288 K – 308 K) were studied at the optimized pH of uranyl ion solution. Except for the adsorbent dose optimization study, all other adsorption studies were performed using 50 mL of uranyl ion solution (50 mg/L) in a temperature controlled shaker bath at 150 rpm. The equilibrium condition corresponded to

12 h contact time. The pH of the medium was adjusted using very small volume of 0.1M HNO_3 and 0.1M NaOH.

2.5 Quantitative estimation of uranium

The concentration of uranium was measured by spectrophotometric method using Arsenazo III as a dye which forms a blue coloured complex with uranium with a characteristic absorption peak at 650 nm. A 0.07% (w/v) arsenazo III reagent was prepared in 3 M perchloric acid. An aliquot of the adsorbate (uranyl ion) was pipette out from the supernatant and mixed with the freshly prepared arsenazo III reagent in 1: 4 volume ratio.[32] The absorbance of the uranyl ion complexed with arsenazo III was measured at 650 nm using Shimadzu UV-1800, and the intensity of the colour of the complex was proportional to the concentration of uranyl ions (Fig. 1).

3. Results and Discussion

3.1 Characterization of NH_3-GO

The synthesis of NH_3-GO involved two steps, i.e., oxidation of graphite to graphene oxide (GO) and subsequent reduction by ammonia to produce ammonia modified graphene oxide (NH_3-GO). The products formed at each stage, i.e., GO and NH_3-GO was monitored by XRD (Fig. 2). The crystalline nature of GO was evident from the intense peak recorded at $2\theta = 8.9°$ (d = 9.67 Å), which corresponded to (002) plane. A lesser intensity peak was observed at 29.67° (3.007 Å) corresponding to (100) plane and our results were in good agreement with those reported for GO,[33] and hence confirmed the synthesis of GO by modified Hummer's method. Further, the modification of GO by ammonia led to decrease in the d-spacing, (d = 3.63 Å) at $2\theta = 24.5°$ corresponding to the (002) plane and a weaker peak at $2\theta = 43.088°$ (d = 2.09 Å) for (100) plane.

A layered structure of the as synthesized NH_3-GO was confirmed from transmission electron microscopy (Fig. 3).

The Raman spectroscopy of NH_3-GO was performed to investigate the effect of modification of GO by ammonia. The Raman spectrum of both GO and NH_3-GO is given in Fig. 4, which revealed two prominent peaks at 1350 cm^{-1} and 1582 cm^{-1}, corresponding to the D and G band, respectively.[34] The D band originates from the stretching vibration of sp^3 carbon atoms which is associated with order/disorders of the system.[35] While the G band (an indicator of staking structure) originates from the stretching vibrations of sp^2 carbon atoms and it is associated with first order scattering of the E_{2g} mode.[36] The ratio of the intensities of these D and G bands, i.e. I_D/I_G can be used as an indicator of number of layers in a graphene sample and its overall staking behaviour. The I_D/I_G value was determined as 0.91 for GO and 1.01 for NH_3-GO. Higher I_D/I_G value indicate higher degree of exfoliation/disorder, which is attributable to the incorporation of N-atoms in the aromatic graphene network of NH_3-GO.[37]

The functional groups in GO and NH_3-GO were analysed by FT-IR spectroscopy. The FT-IR spectrum of GO revealed characteristic peaks at around 3420 and 1736 cm^{-1} corresponding to O-H and C=O stretching frequencies of the -COOH group, respectively (Fig. 5). The peaks corresponding to aromatic C=C bending, phenolic C-O stretching and epoxy C-O-C stretching were identified at 1637, 1222 and 1050 cm^{-1}, respectively. In the case of NH_3-GO, the IR peak at 3420 cm^{-1} diminished significantly indicating the loss of either or both O-H group and intercalated water molecules. The peak at 1736 cm^{-1} was not identified, while a new peak was observed at 1571 cm^{-1} along with a weak band at 1624 cm^{-1}. These two peaks are attributed to the N-H bending and C=O stretching of primary amide group. The indication of amide bond formation in our NH_3-GO was consistent with reported literature.[38] In addition, the FT-IR

signature of basal graphene plane was observed in the range 900-600 cm^{-1} for both GO and NH_3-GO. It may be persuaded from FT-IR studies that amide groups are likely to be formed due to interaction of liquid ammonia with graphene oxide as against pyrazole formation in the hydrazine hydrate induced reduction of graphene oxide.[30]

3.2. Comparative study of uranyl ion adsorption capacities of NH_3-GO, GO

The uranyl ion adsorption capacity at equilibrium condition (q_e) was determined from the following expression:

$$q_e = \frac{C_o - C_e}{m} \times V$$

Where C_o and C_e represent the concentrations of uranyl ions in mg/L in the solution at t = 0 and at equilibrium time respectively, m is the mass of adsorbent (in g) and V is the volume of solution (in L). The q_e of uranyl species on the surfaces of as synthesized graphene oxide and NH_3-GO were studied over a pH range between 2 and 9 and the results are given in Fig. 6a. It was evident that the q_e values were significantly higher for graphene oxide over the entire pH range and our results were consistent with reported literature.[39,40] The adsorption pheneomenon depends on various parameters including the surface charge on adsorbent, which is pH dependent. The zeta potentials were measured over pH range between 2 and 9 for both GO and NH_3-GO and results are presented in Fig. 6b. The pH_{ZPC} was determined to be 3.66 for NH3-GO (Fig. 6b). The maximum q_e for NH_3-GO was obtained at pH 6 and pH 7 where the zeta potential values were more than -25 mV, which is for suitable for electrostatic interaction with positively uranyl ions. However, in the case of pH > 7 the adsorption phenomenon was hindered for NH_3-GO. At alkaline pH, uranium species are reported to exist as stable and soluble neutral carbonate

complexes which are not favourable for electrostatic interaction with negatively charged surface of NH_3-GO nanosheets.[41]

The suitability of NH_3-GO as an adsorbent would definitely depend on the selectivity of uranyl ion adsorption in presence of common interfering cations and anions which are commonly present in ground water. The common interfering cations considered in this study were Ca^{2+} (75 mg/L), Mg^{2+} (30 mg/L), K^+ (50 mg/L), Na^+ (200 mg/L), Pb^{2+} (0.1 mg/L), Fe^{2+} (0.3 mg/L) and Zn^{2+} (5 mg/L) and anions like CO_3^{2-} (300 mg/L), HCO_3^- (300 mg/L), Cl^- (250 mg/L) and SO_4^{2-} (200 mg/L), where the concentrations of these interfering species are given in the bracket as per the permissible limits by Bureau of Indian Standards (BIS)[42] and WHO.[3] The q_e values of uranyl ion adsorption on NH_3-GO (at pH 6) were determined for the cases without and with respective interfering ions (Fig. 6c). Similarly, the q_e values of uranyl ion adsorption on GO as adsorbents (at pH 5) were determined for the cases without and with respective interfering ions (Fig. 6c). It was noted that the q_e values of uranyl ion adsorption was significantly affected for all the interfering ions. The decrease in the q_e value was most significant for Ca^{2+}, Mg^{2+} as interfering ions. This is due to the competing nature of the Ca^{2+} /Mg^{2+} and UO_2^{2+} to bind with the active binding sites of the GO. The affinity of cations to bind with GO was substantiated from the negative zeta potential measurements of GO over the pH range between 2 and 9 (Fig. 6b). The negative zeta potential was due to the carboxylate group in the GO. It was however, noted that the q_e value of uranyl ion adsorption were drastically reduced in the presence of anions as interfering agents, e.g., CO_3^{2-}, Cl^- and SO_4^{2-}.The observed decrease in the q_e of uranyl ions for anion interference cannot explained due to electrostatic interaction as it was discussed for cations. It may be remarked that the uranyl ions tend to form anionic complexes, e.g., $UO_2[CO_3]_2^{2-}$, $UO_2Cl_4^{2-}$, $UO_2[SO_4]_2^{2-}$ in the presence of these anions.[43,44] Due to this, the net

available concentration of cationic uranyl ions in the medium is expected to decrease and subsequently account for decrease in the q_e value of adsorption of uranyl ions on GO in presence of these anions.

On the contrary, the q_e value of uranyl ion adsorption on NH3GO was not affected in the presence of Na^+, Mg^{2+}, K^+, Fe^{2+}, Pb^{2+} and Zn^{2+} , HCO_3^-, CO_3^{2-} and SO_4^{2-}. The q_e value of uranyl ion adsorption was mildly affected due Ca^{2+} and Cl^-, where the q_e value was found to reduce by about 30 % in the presence of these interfering ions. Inspite of high q_e values for uranyl ion adsorption on GO, poor selectivity was its major drawback as an adsorbent. From this study, it is also evident that NH_3-GO is a better adsorbent for uranyl ion removal from aqueous medium in the presence of interfering ions. Further studies were performed to understand the mechanism of adsorption of uranyl ions on NH_3-GO at pH 6, at which the positively charged uranyl ion species e.g., UO_2^{2+}, $UO_2(OH)^+$, $(UO_2)_2(OH)_2^{2+}$, $(UO_2)_3O(OH)_3^+$ commonly exist.[12]

3.3 Qualitative studies of NH_3-GO as adsorbents for uranyl ions by SEM-EDX

The FE-SEM image of the pristine NH_3-GO and uranyl ion adsorbed on NH_3-GO are given in Fig. 7a and 7b, respectively. A better contrast was observed for the batch of NH_3-GO adsorbed with uranyl ions owing to the principle of higher secondary electron emission due to interaction of incident electrons with higher atomic number elements. This was also evident from the FE-SEM images recorded using backscattering electrons, where higher order of backscattering occurred from the surface with heavier atoms, e.g., uranium (Fig. 7c) as compared to the pristine batch comprising mostly carbon and hydrogen (Fig. 7d). Further, elemental maps of C, O, N and U and their collective map are given as Fig. 7e-7i, respectively. The adsorption of U on NH_3-GO is reflected from the corresponding EDX spectrum revealing M X-rays of U, shown in Fig. 7j. It

was noted from the elemental maps that the spatial distribution of C was not correlated with that of O. Primarily O distribution was expectedly more pronounced in the periphery of NH_3-GO while C was mainly distributed at the inner region of the image of NH_3-GO structure. This is in good agreement with the proposed structure of graphene oxide where all the oxygen due to carboxyls and carbonyls are located at the edges of graphene oxide.[29,30] The N map, however did not reveal any hotspot, but it was a close resemblance with O map pertaining to amide bond in NH_3-GO. Strikingly, the U map was correlated with those of O and N maps which implied the tentative affinity of uranyl ions with the amide.

3.4 Effect of adsorbent dose, contact time and initial concentration of uranyl ions

The trend of adsorption efficiency and corresponding q_e values of uranyl ions at pH 6 is plotted against adsorbent dose (Fig. 8a). An increase in the adsorption efficiency from 20 % to 84 % was observed with the increased as the amount of adsorbent (NH_3-GO) from 10 mg to 70 mg. This is attributed to the availability of more binding sites and higher surface area for adsorption. However, the q_e trend decreased with increase in the adsorbent dose. The effect of contact time on the adsorption capacity of NH_3-GO was examined using fixed adsorbent dose of 1g/L (amount of adsorbent per volume, where the uranyl ion concentration was fixed) at 298 K. Detailed analysis revealed 57 % adsorption of uranyl ions in the first 60 min and equilibrium condition was achieved in the 3 h (Fig. 8b). For subsequent studies, 4 h contact time was used for determining the q_e value of uranyl ions by NH_3-GO. The effect of initial concentration of uranyl ion on q_e was assessed for the batches of initial uranyl ion concentration ranging between 5 mg/L and 100 mg/L. The corresponding measured q_e values were between 4.5 mg/g and 65.65 mg/g (Fig. 8c). The increase in the q_e values with increase in the uranyl ions concentrations is

attributable to enhanced frequency of collision between the adsorbate and adsorbent. It should be mentioned here that all the subsequent adsorption studies were performed for initial uranyl ion concentration of 50 mg/L, for which the q_e corresponded to 40.10 mg/g.

3.5 Adsorption Mechanism

3.5.1 Adsorption isotherms

The adsorption of uranyl ions on NH_3-GO nanosheets was studied at pH 6 and at 298 K in terms of Freundlich, Langmuir and Temkin adsorption isotherms. The Freundlich isotherm is appropriate for heterogenous surface and the linear form of Freundlich isotherm is represented as,

$$\log q_e = \log K_F + \frac{1}{n} \log C_e$$

Here K_F is the Freundlich isotherm constant (in mg/g), which is an approximate indicator of adsorption capacity and *1/n* is related to the heterogeneity parameter of the sorbent and indicates strength of adsorption in the adsorption process.[45] The parameters K_F and n are characteristic of the sorbent-sorbate system and were determined respectively from the intercept and the slope of the linear fit of the plot of *log* q_e and *log* C_e (R^2= 0.960), given in Fig. 9a. The value of K_F was also large (9.17 mg/g), which implied a strong adsorption affinity of uranyl ions on the NH_3-GO adsorbent. The value of *n* provides information if the adsorption process is independent of concentration of sorbate (if n = 1), or the process is due to cooperative adsorption (1/n >1) or otherwise the adsorption is normal (1/n <1).[46] In the case of uranyl ion adsorption on NH_3-GO, 1/n = 0.607 indicated normal adsorption process owing to heterogeneity in the sorbent prevailing at working pH 6.

The adsorption data was studied with respect to Langmuir adsorption isotherm model which represents equilibrium distribution of metal ions between solid and liquid phase and quantitatively describes the maximum monolayer coverage on the surface of the adsorbent. The model assumes that the surface of the adsorbent contains a finite number of identical sites with uniform energies of adsorption onto the surface and does not consider any transmigration of adsorbate across the surface of the adsorbent.

The linear form of Langmuir adsorption isotherm is given as,[47]

$$\frac{C_e}{q_e} = \frac{1}{k_L q_{max}} + \frac{C_e}{q_{max}}$$

and the equilibrium parameter is $$R_L = \frac{1}{1+(1+k_L C_o)}$$

Here q_e (in mg/g) and C_e (mg/L) are the adsorption capacity and the concentration of uranyl ions at equilibrium condition, respectively; k_L is the Langmuir isotherm constant (L/mg) and q_{max} (mg/g) is the maximum adsorption capacity of the adsorbent (NH_3-GO) and C_o is the initial concentration of uranyl ions. The R_L value, which is separation factor and indicates the nature of adsorption, is unfavourable if $R_L > 1$; irreversible if $R_L = 0$; linear if $R_L = 1$ and the adsorption is favourable if $0 < R_L < 1$. The values of q_{max} and k_L were computed from the slope and intercept, respectively of the plot of C_e/q_e vs. C_e, given in Fig. 9b. The data fitting with Langmuir isotherm model linear (R^2 = 0.993) indicating that the adsorption of uranyl ions on NH_3-GO favoured Langmuir model, which assumes monolayer adsorption without any chemical interaction between sorbate and the sorbent. Further the value of k_L was determinied as 0.115 and correspondingly the R_L values were found in the range between 0.285 and 0.481, which implied that the adsorption of uranyl ions in the chosen concentration range (5 mg/L and 100 mg/L) was favourable. The maximum monolayer adsorption capacity (q_{max}) of NH_3-GO for uranyl ion

sorption was derived to be 80.13 mg/g, which is larger than the q_{max} reported for several conventional adsorbent reported for adsorption of uranyl ions (listed in Table 1). The Langmuir adsorption isotherm data predicts that the q_e increases with an increase in temperature and the analogous behaviour is ascribed by the adsorption capacity (K_F) as well. Notably, adsorption of uranyl ions on NH_3-GO was linearly fitted by both Freundlich model and Langmuir model which might indicate that both physisorption as well as chemisorption processes might occur simultaneously or alternately.[48]

Further insight of adsorption process was obtained from the studies on Temkin isotherm model, which assumes that the adsorption is due to chemical interaction where that the heat of adsorption decreases linearly and not logarithmic with the surface coverage due to adsorbate – adsorbent interactions. The Temkin model is given as,[49]

$$q_e = \frac{RT}{b} ln\, k_T + \frac{RT}{b} ln\, C_e$$

Where

$$\frac{RT}{b} = B$$

where q_e and C_e are same as defined earlier, R is universal gas constant, b is the Temkin isotherm constant and B is the Temkin constant related to heat of adsorption (J/mol) and k_T is the Temkin isotherm equilibrium constant (L/g). The plot of q_e vs lnC_e is given in Fig. 9c and a linear fit was obtained (R^2 = 0.975), indicating that the adsorption of uranyl ions on the adsorbent was reasonably in good agreement with Temkin model. The parameter B was determined to be 15.006, which is consistent with the adsorption phenomenon governed by chemical processes.

3.5.2 Thermodynamic studies

The effect of temperature on the adsorption of uranium ions on NH_3-GO was studied at three different temperatures i.e. 288 K, 298 K and 313 K. The q_e value increased with increase in the temperature which indicated that adsorption is endothermic in nature. The thermodynamic parameters, e.g., the change in enthalpy ($\Delta H°$) and entropy ($\Delta S°$) were calculated to be +35.087 kJ/mol and +126.83 J/mol, respectively from the intercept and slope of the linearly fitted (R^2 = 0.974) plot of lnK_d vs $1/T$. The positive values of $\Delta H°$ and $\Delta S°$ indicated that the adsorption process was endothermic and associated with increased randomness at the interface of adsorbate-adsorbent and the results are consistent with adsorption isotherm. Similar thermodynamic property was also reported for uranyl ion adsorption in graphene oxide adsorbent.[40] Notably, the magnitude of the $\Delta H°$ was higher than that of a typical physisorption and was near to the range satisfying chemisorptions process. The $\Delta G°$ values for the respective temperatures (calculated using the expression $\Delta G° = \Delta H° - T\Delta S°$) were -1.489, -2.759 and - 4.664 kJ/mol at 288, 298 and 313 K, respectively. The negative $\Delta G°$ value implied that the adsorption of uranyl ions on to NH_3-GO nanosheets was favourable and was of spontaneous in nature. From the thermodynamic studies and isotherm models it may be surmised that the adsorption of uranyl ions on NH_3-GO is based on combination of both chemisorption and physisorption process.

3.5.3 Kinetic studies

Adsorption is a physicochemical process which involves transfer of adsorbent from solution phase to the surface of the adsorbent. The adsorption kinetics provides valuable insights about the reaction pathways and adsorption mechanism. The kinetic study also describes the solute uptake rates and can be best explained in terms of pseudo first order, pseudo second order and

intraparticle diffusion model.[50] The linear form of pseudo-first order kinetics model is represented as,

$$\log(q_e - q_t) = \log q_e - \frac{k_1}{2.303}t$$

Where q_e and q_t represents the adsorption capacities at equilibrium condition and at any specific time *t,* respectively; and k_1 is the pseudo first order rate constant. The linear fit of the plot of log (q_e- q_t) vs. time (t) was poorly correlated (R^2= 0.952), as shown in Fig. 11a. It may be inferred that the adsorption of uranyl ions on NH_3-GO was not based on pseudo first order kinetics and hence the adsorption was not a diffusion controlled.

The pseudo second order kinetic model in linear form is represented as,

$$\frac{t}{q_t} = \frac{1}{k_2 q_e^2} + \frac{1}{q_e}t$$

Where k_2 is second order rate constant; while q_e and q_t are same as defined above for the pseudo-first order kinetics equation. The linear fit of the plot of t/q_t vs t revealed high correlation coefficient (R^2 = 0.994), as shown in Fig. 11b. This suggested that the adsorption of uranyl ions on NH_3-GO followed pseudo second order model, which is based on the assumption that the rate limiting step may be due to chemisorption involving valency forces through sharing or exchange of electrons between NH_3-GO and uranyl ions. This is likely to be attributed to chemical affinity of uranyl ions with the amides of NH_3-GO. The q_e and k_2 values, determined from the slope and the intercept of the plot, were 41.7 mg/g and 1.167×10^{-3}, respectively. The q_e value determined from the pseudo-second order kinetics model was in good agreement with the experimental q_e (40.10 mg/g). The magnitude of the k_2 was small, which indicated that the rate of uranyl uptake decreases with time. It was noted from literature that the adsorption of uranyl ions studied in

graphene oxide or reduced graphene oxide as adsorbent also followed pseudo-second order kinetics.[39,40,51]

There was a strong indication from pseudo-first order and pseudo-second order kinetics model that the adsorption of uranyl ions on NH_3-GO was not due to diffusion. In order to ascertain this, the adsorption data was studied in view of intraparticle diffusion model given as, [52]

$$q_t = k_i t^{1/2} + C$$

Where K_i is the intraparticle diffusion rate constant (mg g^{-1} $min^{0.5}$) and C is the intercept. The plot of q_e vs $t^{1/2}$ revealed two linear characteristics as indicated in the Fig. 11c, and their respective correlation coefficient values (R^2) were 0.996 and 0.969, respectively. Since the region I of the plot did not pass through the origin, it may be concluded that adsorption of uranyl ions on NH_3-GO was not based on diffusion mechanism.[53] The second region of the intraparticle diffusion model is attributable to final equilibrium stage.

3.6 Desorption and re-usability of the NH3-GO adsorbent

The best result for regenerating spent NH_3-GO as adsorbent was achieved by washing with 1 M HNO_3 at 50 °C for 60 min. The concentration of the desorbed uranyl ion was determined by arsenazo (III) dye method and 99. 6 % of adsorbed uranyl ions were desorbed in the first cycle. The NH_3-GO was washed with 1 M NH_4OH and conditioned to pH 6. The adsorption efficiency of uranyl ions was 83.55 % in the second cycle and subsequent desorption of uranyl ion was 98.70 %. Similarly in the 3rd cycle, the adsorption efficiency of uranyl ions was 82.16% and the subsequent desorption was 98.40 %. The results of our desorption study is consistent with the literature report.[54] From these results, it was inferred that NH_3-GO is an efficient adsorbent and

can be re-used multiple times for removal of uranyl ions from aqueous medium without compromising the efficiency of uranyl ion adsorption.

It may be surmised that the modification of graphene oxide by ammonia led to amidation of carboxylic acid group due to which the adsorption of uranyl ions followed a combination of chemisorption as well as physisorption mechanisms which were consistent with the adsorption isotherm models and adsorption kinetics models studied here. The maximum adsorption capacity of uranyl ions by NH_3-GO (i.e., q_{max}) was 80.13 mg/g at pH 6, which was significantly higher than most of the common types of adsorbents reported for uranyl ions as given in Table 1.[55-72] Notably graphene oxide based adsorbents and those belonging to clay type adsorbents listed in Table 1 revealed very high q_{max} value, but their selectivity towards uranyl ion adsorption is not suitably addressed.[2,20,21,40,54,73-76] In the present study, the q_e for GO was though found to be greater than the q_e for NH_3-GO, but better selectivity for adsorption of uranyl ion is the salient advantage of NH_3-GO adsorbent. Further studies would be required to increase the number of binding sites in NH_3-GO by develop suitable chemical methods to functionalize of the adsorbent surface for improving the selectivity of uranyl ion species.

4. Conclusions

Ammonia modified graphene oxide (NH_3-GO) has been successfully synthesised and its application as an adsorbent for uranyl ions has been systematically studied. The adsorption isotherm studies, kinetic studies and thermodynamic studies indicated a dual mechanism of chemisorption and physisorption owing to heterogenous binding sites in NH_3-GO. The necessity for modification of graphene oxide has been explicitly demonstrated here. Though the adsorption capacity of graphene oxide for uranyl ions was high, but it revealed poor selectivity towards

uranyl ion adsorption in the presence of cationic and anionic interfering species that are commonly present in ground water. On the other hand, NH_3-GO revealed better selectivity towards adsorption of uranyl ions with respect to interference from the cations and anions, which was attributed to amide functionalization of graphene oxide. In addition, maximum adsorption of uranyl ions by NH_3-GO was achieved at neutral (pH 7) or mildly acidic condition (pH 6), which would allow NH_3-GO to be suitable for uranium removal in contaminated water.

Acknowledgment

Swati Verma wishes to thank Council for Scientific and Industrial Research (CSIR), Government of India for providing Senior Research Fellowship. The authors also thank Institute Instrumentation Centre of IIT Roorkee for providing necessary instrumentation facility.

References

1. G.H. Wang, J.S. Liu, X.G. Wang, Z.Y. Xie and N.S. Deng, *J. Hazard. Mater*. 2009, 168, 1053-1058.
2. T.S. Anirudhan and S. Rijith, *J. Environ. Radioact.* 2012, 106, 8-19.
3. WHO, Guidelines for Drinking Water Quality, 3rd ed., WHO, (2003).
4. U.S. EPA, EPA Integrated Risk Information System (IRIS) Electronic Database U.S. Environmental Protection Agency, Washington, DC (1996).
5. Nakajima and T. Sakaguchi, *J. Radioanal. Nucl. Chem.* 1999, 242, 623-626.
6. X. Sun, X. Huang, X.P. Lian and B. Shi, *J. Hazard. Mater.* 2010, 179, 295-302.
7. V.V. Ranade, V.M. Bhandari, Industrial Wastewater Treatment, Recycling and Reuse, 2014, Elsevier, Oxford UK.
8. T.E. Milja, V.S. Krupa and T.P. Rao, *RSC Adv*. 2014, 4, 30718-30724.
9. G. Crini, *Bioresour. Technol*. 2006, 97, 1061-1085
10. S. Zhang, W. Xu, M. Zeng, J. Li, J. Li, J. Xu and X. Wang, *J. Mater. Chem. A*. 2013, 1, 11691-11697.
11. S. Zhang, M. Zeng, J. Li, J. Li, J. Xu and X. Wang, *J. Mater. Chem. A.* 2014, 2, 4391-4397.
12. Z.H. Huang, X. Zheng, W. Lv, M. Wang, Q.H. Yang and F. Kang, *Langmuir* 2012, 27, 7558–7562
13. Z. Li, F. Chen, L. Yuan, Y. Liu, Y. Zhao, Z. Chai and W. Shi, *Chem. Eng. J.* 2012, 210, 539-546.
14. S. Zhang, J. Li, X. Wang, Y. Huang, M. Zeng, and J. Xu, *Appl. Mater. Interfaces.* 2014, 6, 22116-22125

15. S. Zhang, J. Li, X. Wang, Y. Huang, M. Zeng, and J. Xu, *J. Mater. Chem. A*. 2015, 3, 10119-10126.

16. M. Yusuf, F.M. Elfghi, S.A. Zaidi, E.C. Abdullah, and M.A. Khan, *RSC. Adv*. 2015, 5, 50392-50420.

17. S. Park and S.S. Ruoff, *Nat Nanotechnol*. 2009, 4, 217–224.

18. R. Sitko, P. Janik, B. Zawisza, E. Talik, E. Margui and I. Queralt, *Anal. Chem.* 2015, 87, 3535-3542

19. Y. Shen, B. Chen, *Environ. Sci. Technol.* 2015, 49, 7364–7372.

20. S. Chen, J. Hong, H. Yang and J. Yang, *J. Environ.Radioact*. 2013, 126, 253-258

21. Y. Zhao, J. Li, S. Zhang, H. Chen and D. Shao, *RSC Adv*. 2013, 3, 18952-18959.

22. S. Kumar, R.R. Nair, P.B. Pillai, S.N. Gupta, M.A.R. Iyengar and A.K. Sood, *ACS Appl. Mater. Interfaces*, 2014, 6, 17426 – 17436

23. S. Kobayashi, M. Tokunoh, T. Saegusa and F. Mashio, *Macromolecules*, 1985, 18, 2357-2361

24. G. Benay, G. Wipff, *J. Phys. Chem. B* 2013, 117, 7399-7415

25. S. Park, J. An, J.R. Potts, A. Velamakanni, S. Murali, Rodney and S. Ruoff, *Carbon*. 2011, 49, 3019-3023.

26. S.K. Singh, M.K. Singh, P.P. Kulkarni, V.K. Sonkar, J.J.A. Gracio and Debabrata Dash, *ACS Nano*, 2012, 6, 2731-2740

27. A. Yang, J. Li, C. Zhang,W. Zhang and N. Ma, *Appl. Surf. Sci.* 2015, 346, 443-450.

28. S. Dutta, C. Ray, S. Sarkar, M. Pradhan, Y. Negishi and T. Pal, *ACS Appl. Mater. Interfaces*, 2013, 5, 8724-8732.

29. D.R. Dreyer, S. Park, C.W. Bielawski and R.S. Rouff, *Chem. Soc. Rev.*, 2010, 39, 228-240

30. S. Park, Y. Hu, J.O. Hwang, E.-S. Lee, L.B. Casabianca, W. Cai, J. R. Potts, H.-W. Ha, S. Chen, J. Oh, S.O. Kim, Y.-H. Kim, Y. Ishii and R.S. Ruoff, *Nat. Commun.* 2012,
31. W.S. Hummers and R.E. Offeman, *J. Amer. Chem. Soc.* 1958, 80, 1339-1341.
32. L. Jauberty, N. Drogat, J.L. Decossas, V. Delpech, V. Gloaguen and V. Sol, *Talanta*. 2013, 115, 751-754.
33. S. Yang, W. Yue, D. Huang, C. Chen, H. Lin and X. Yang, *RSC Adv*. 2012, 2, 8827–8832.
34. M.A. Pimenta, G. Dresselhaus, M.S. Dresselhaus, L.G. Cancado, A. Jorio and R. Saito, *Phys. Chem. Chem. Phys.* 2007, 9, 1276-1290.
35. J. Wang, Z.M. Chen and B.L. Chen, *Environ. Sci. Technol*. 2014, 48, 4817–4825.
36. J.F. Shen, Y.Z. Hu, M. Shi, X. Lu, C. Qin, C. Li and M.X. Ye, *Chem. Mater*. 2009, 21, 3514–3520
37. A. Das, B. Chakraborty and A. K. Sood, *Bull. Mater. Sci.,* 2008, 31, 579–584
38. L. Lai, L. Chen, D. Zhan, L. Sun, J. Liu, S.H. Lim, C.K. Poh, Z. Shen and J. Lin, *Carbon*, 2011, 49, 3250-3257
39. A.Y. Romanchuk, A.S. Slesarev, S.N. Kalmykov, D.V. Kosynkin and J.M. Tour, *Phys. Chem.. Chem.. Phys,* 2013, 15, 2321-2327.
40. G. Zhao, T. Wen, X. Yang, S. Yang, J. Liao, J. Hu, D. Shao and X. Wang, *Dalton Trans.* 2012, 41, 6182-6188.
41. I.A. Katsoyiannis And A.I. Zouboulis, *Desalin. Water. Treat*. 2013, 51, 2915-2925.
42. Indian Standard for Drinking Water-Specification IS 10500:1991
43. G. Bernhard, G. Geipel, V. Brendler and H. Nitsche, *J. Alloys Compd.* 271-273, 201-205
44. M.-O. Sornein, C. Cannes, C. Le Naour, G. Lagarde, E. Simoni, and J.-C. Berthet, *Inorg. Chem*. 2006, 45, 10419-10421.

45. S.V. Mohan, and J. Karthikeyan, *Environ. Pollut.* 1997, 97, 183-197.

46. S. Goldberg. Chemical Processes in Soils Eds. M.A. Tabatabai, D.L. Sparks, Soil Science Society Of America, USA, 2005,Vol. 8, Ch 10, pp 489-517.

47. I. Langmuir, *J. Am. Chem. Soc*. 40, 1918, 1361-1403.

48. A. Dabrowski, *Adv. Colloid Interface Sci.* 2001, 93, 135-224.

49. M.J. Tempkin, and V. Pyzhev, *Acta Phys. Chim. USSR*, 1940, 12, 327–356.

50. Y.S. Ho and G. Mckay, *Process Biochem.* 1999, 34, 451 – 465.

51. P. Zong, S. Wang, Y. Zhao, H. Wang, H. Pan and C. He, *Chem. Eng. J*. 2013, 220, 45-52.

52. F.-C. Wu , R.-L. Tseng and R.-S. Juang, *Wat. Res.* 2001, 35, 613–618,

53. H.K. Boparai, M. Joseph and D.M. O'Carroll, *J. Hazard. Mater.* 2011, 186, 458-465.

54. W. Cheng, M. Wang, Z. Yang, Y. Sun and C. Ding, *RSC Adv.* 2014, 4, 61919-61926.

55. L.M. Camacho, S. Deng, and R.R. Parra, *J. Hazard. Mater*. 2010, 175, 393-398.

56. W. Um, S. Mattigod, R.J. Serne, G.E. Fryxell, D.H. Kim and L.D. Troyer, *Water Res.* 2007, 41, 3217 – 3226.

57. D. Zhao, X. Wang, S. Yang, Z. Guo and G. Sheng, *J. Environ. Radioact*. 2012, 103, 20-29.

58. A. Mellah, S. Chegrouche and M. Barkat, *J. Colloid Interface Sci*. 2006, 296, 434–441.

59. Y. Sun, S. Yang, G. Sheng, Z. Gua, X. Tan, J. Xu and X. Wang, *Sep. Purif. Technol.* 2011, 83, 196-203.

60. S. Sadeghi, H. Azhdari, H. Arabi, and A.Z. Moghaddam, *J. Hazard. Mater*. 2012, 215-216, 208–216.

61. R. Han, W. Zou, Y. Wang and L. Zhu, *J. Environ. Radioact*. 2007, 93, 127-143.

62. I.I. Fasfous and J.N. Dawoud, *Appl. Sur. Sci.* 2012, 259, 433– 440.

63. R. Leal and M. Yamaura, *Int. J. Nucl. Energ. Sci. Technol*. 2011, 6, 1–7.

64. R. Qadeer, J. Hanif, M. Saleem and M. Afzal, *J. Radioanal. Nucl. Chem. Lett*., 1992, 165(4), 243-253.

65. Y. Sun, S. Yang, G. Sheng, Z. Gua and X. Wang, *J. Environ. Radioact.* 2012, 105, 40-47.

66. D. Shao, Z. Jiang, X. Wang, J. Li and Y. Meng, *J. Phys. Chem. B. Lett.* 2009, 113, 860- 864.

67. D. Shao, J. Hu and X. Wang, *Plasma Processes and Polymers*, 2010, 7, 977 – 985.

68. O. Hazer and S. Kartal, *Talanta*. 2010, 82, 1974–1979.

69. F.L. Fan, Z. Qin, J. Bai, W.D. Rong, F.Y. Fan, W. Tian, X.L. Wu and L. Zhao, *J. Environ. Radioact.* 2012, 106, 40–46.

70. M. Wazne, X. Meng, G.P. Korfiatis and C. Christodoulatos, *J. Hazard. Mater*. 2006,136, 47-52.

71. G. Tian, J. Geng, Y. Jin, C. Wang, S. Li, Z. Chen, H. Wang, Y. Zhao and S. Li, *J. Hazard. Mater.* 2011, 190, 442-450.

72. G.H. Wang, J.S. Liu, X.G. Wang, Z.Y. Xie and N.S. Deng, *J. Hazard. Mater*. 2009, 168, 1053-1058.

73. T.S. Anirudhan, J.R. Deepa and Binusreejayan, *Chem. Eng. J*. 2015, 273, 390–400.

74. H. Cheng, K. Zeng and J. Yu, *J. Radioanal. Nucl. Chem*. 2013, 298, 599–603.

75. D. Shao, G. Hou, J. Lli, T. Wen, X. Ren and X. Wang, *Chem. Eng. J*. 2014, 255, 604-612.

76. L. Tan, Y. Wang, Q. Liu, J. Wang, X. Jing, L. Liu, J. Liu and D. Song, *Chem. Eng. J*. 2015, 259, 752-760.

FIGURE CAPTION

Fig. 1 (a) UV-visible spectrum of uranyl ion complexed with arsenazo III and (b) calibration plot of the absorbance of arsenazo(III)-uranium complex with the concentration of uranyl ions.

Fig. 2 X-ray diffractogram of graphene oxide (GO) and ammonia modified graphene oxide (NH_3-GO)

Fig. 3 Representative TEM image showing formation of ammonia modified nanosheets (NH_3-GO)

Fig. 4 Raman spectra of GO and NH_3-GO showing G and D bands.

Fig. 5 FT-IR spectra of graphene oxide (GO) and NH_3-GO showing modification of COOH group in GO to $CONH_2$ group in NH_3-GO.

Fig. 6 (a) Effect of pH on q_e values; (b) effect of pH on zeta potential values and (c) effect of interfering ions on uranyl ions adsorption by GO and NH_3-GO.

Fig. 7 FE-SEM images of (a) pristine NH_3-GO; (b) uranyl ion bound NH_3-GO; (c) backscattered electron image of uranyl ion bound NH_3-GO; (d) backscattered electron image of NH_3-GO; (e) spatial distribution of carbon; (f) spatial distribution oxygen; (g) spatial distribution nitrogen ; (h)spatial distribution uranium; (i) elemental mapping of the surface of NH_3-GO after adsorption of uranyl ions and (j) EDAX spectrum of uranyl ions adsorbed NH_3-GO.

Fig. 8 (a) Effect of adsorbent dose on q_e values and % adsorption of uranium by NH_3-GO; (b) effect of contact time on q_e values of uranyl ion adsorption by NH_3-GO and (c) effect of initial concentration of uranium ions on the q_e values of NH_3-GO.

Fig. 9 Adsorption of uranyl ions on NH_3-GO as modelled by (a) Freundlich adsorption Isotherm (b) Langmuir adsorption isotherm (c) Temkin adsorption isotherm.

Fig. 10 Showing linear relationship between ln k_d vs 1/T using Vant Hoff equation.

Fig. 11 The adsorption of uranyl ions on NH_3-GO fitted with (a) Pseudo first order kinetic model and (b) pseudo second order kinetic model and (c) intraparticle diffusion model.

TABLE CATION

Table.1 Consolidated list of adsorbents used for adsorption of uranyl ions from aqueous medium.

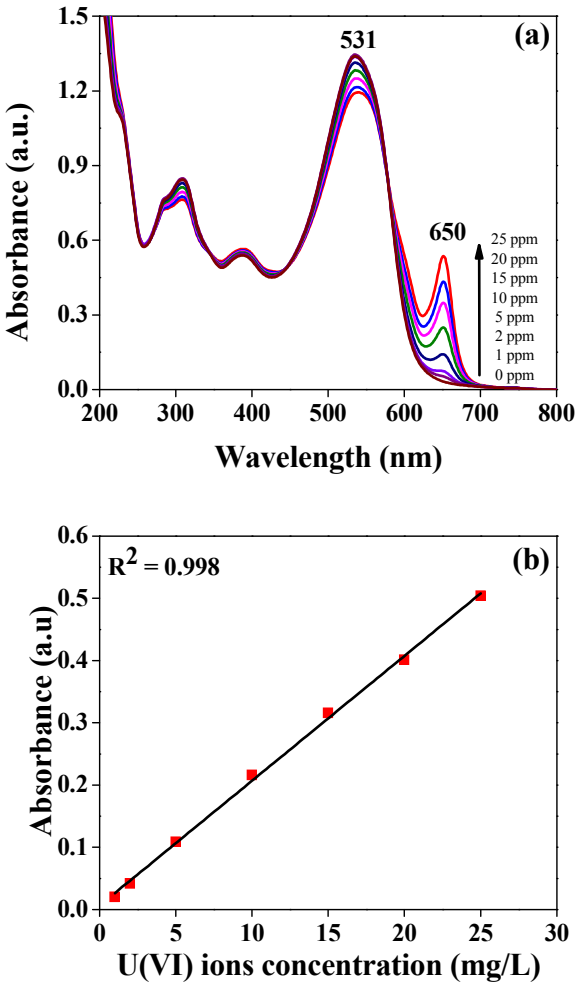

Fig. 1

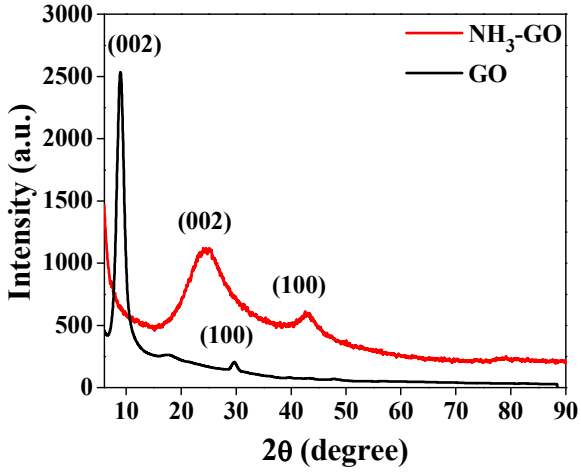

Fig. 2

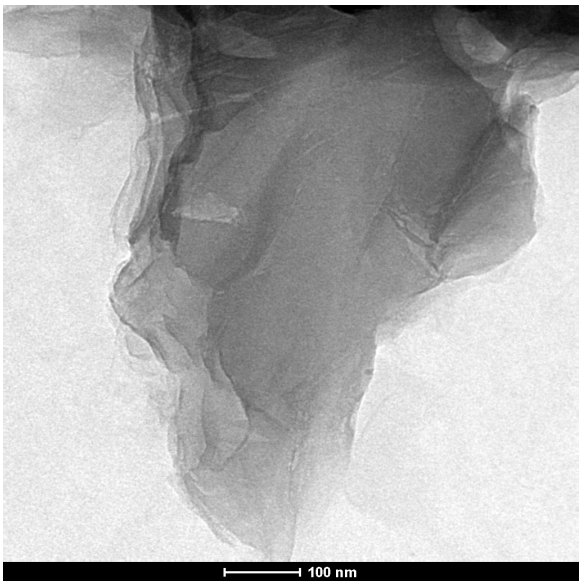

Fig. 3

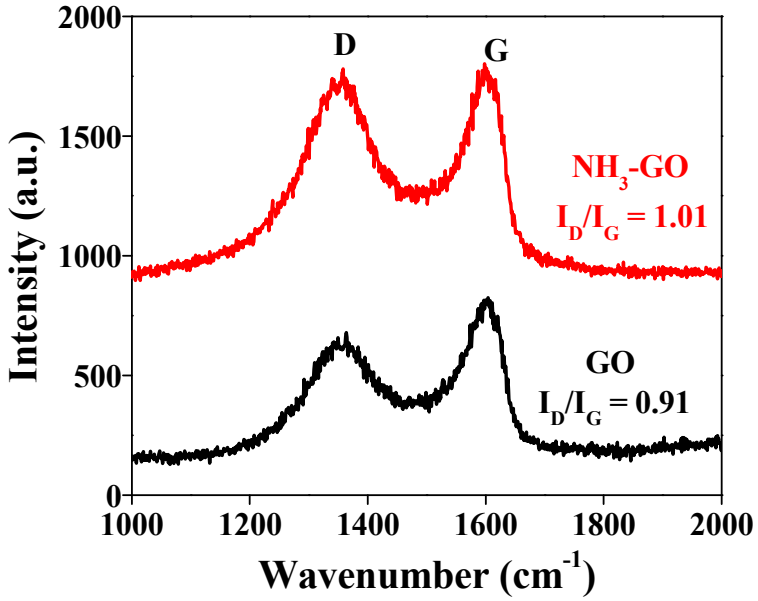

Fig. 4

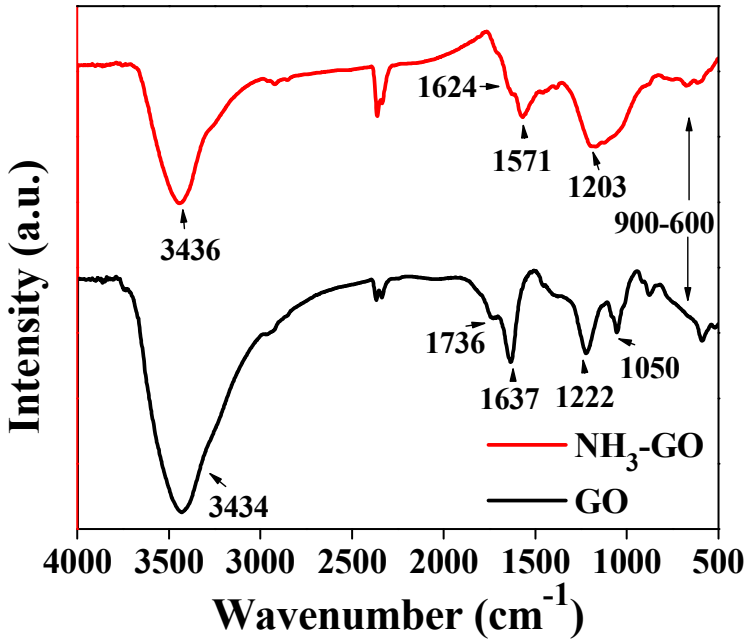

Fig. 5

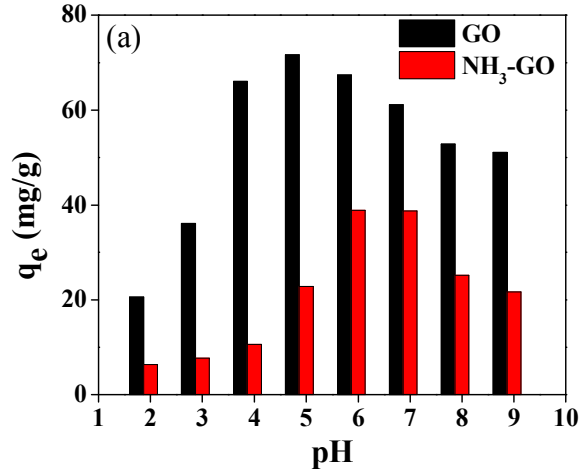

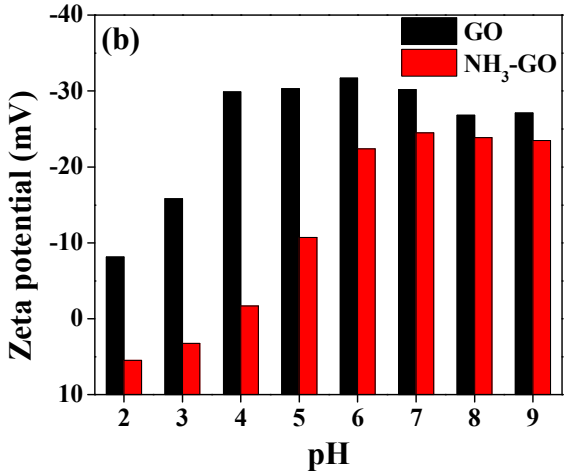

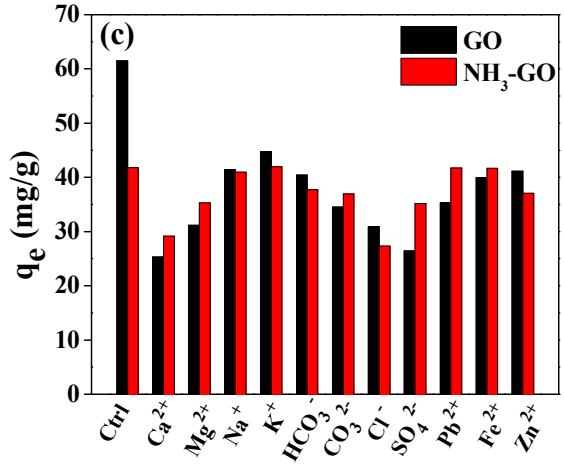

Fig. 6

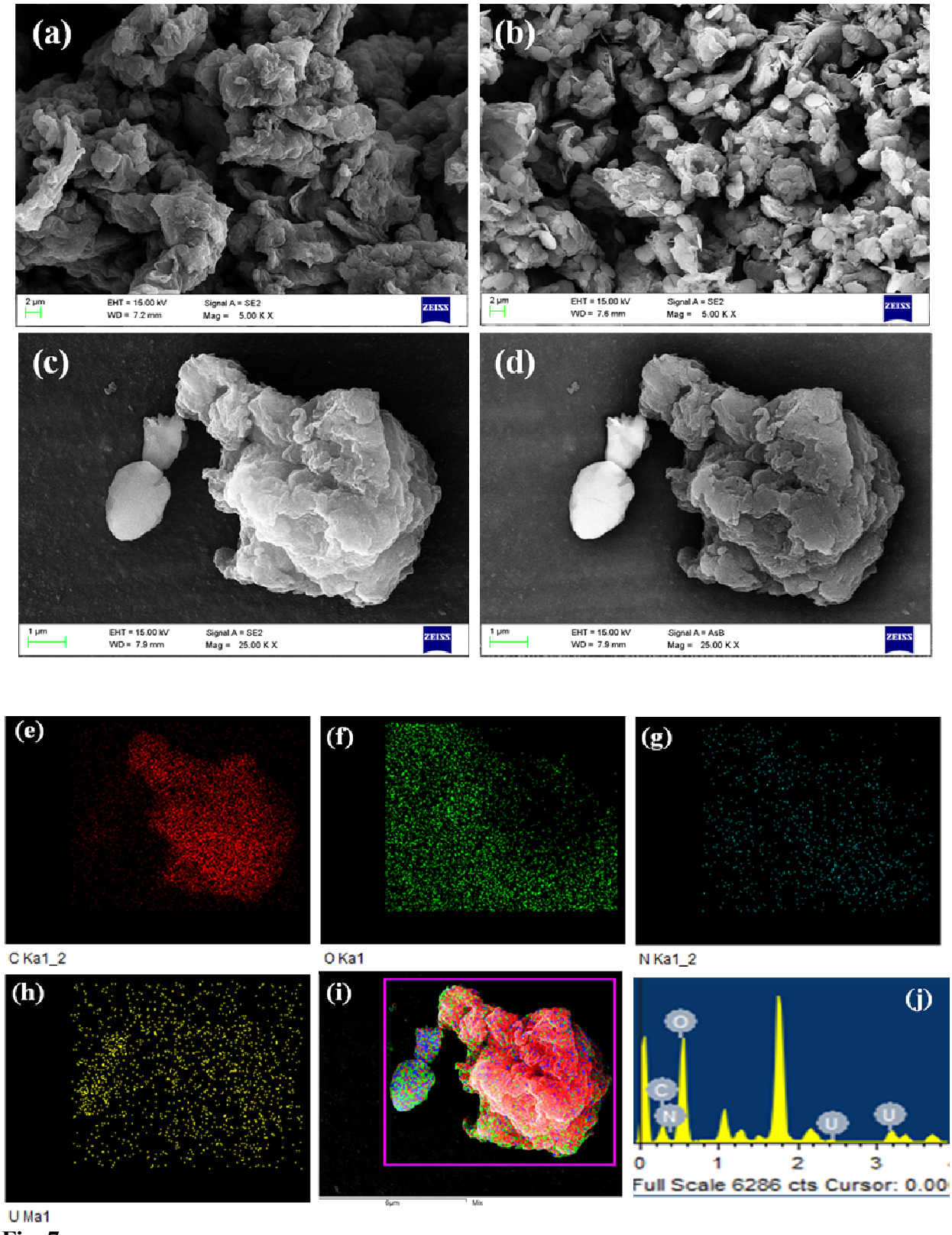

Fig. 7

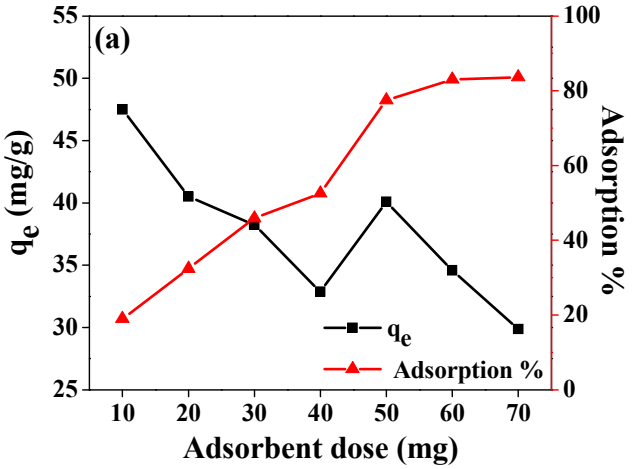

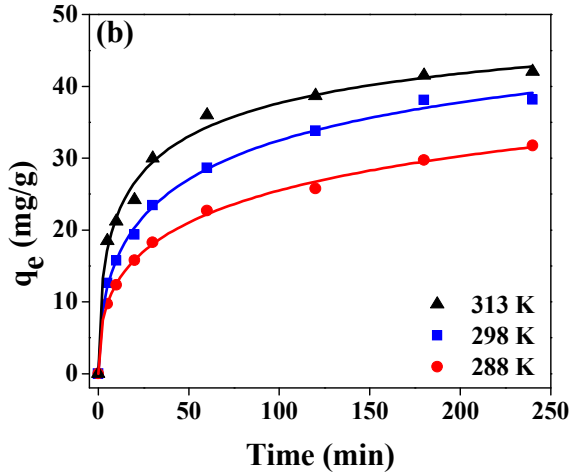

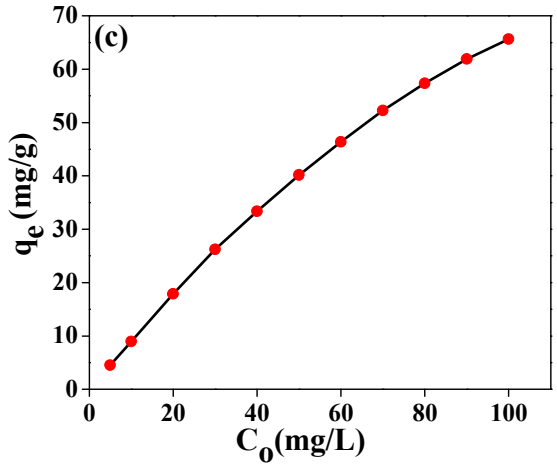

Fig.8

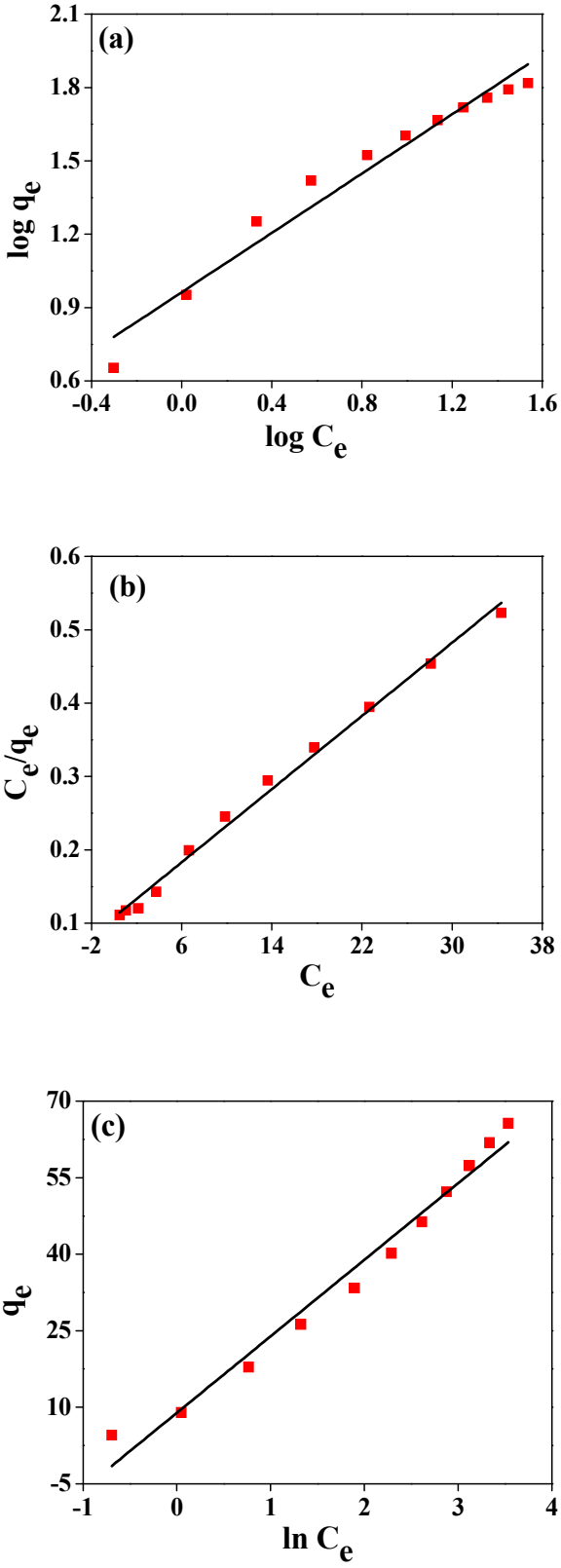

Fig. 9

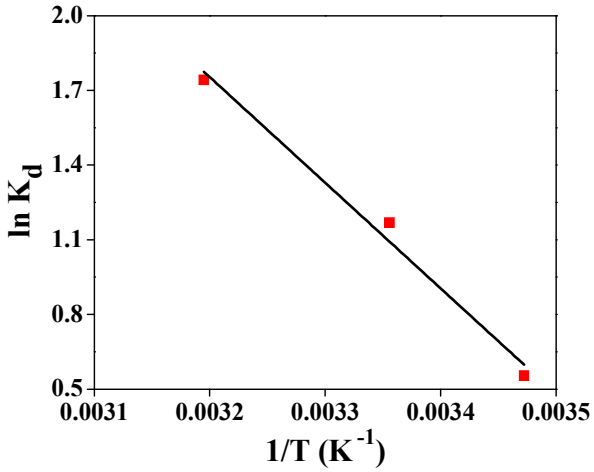

Fig. 10

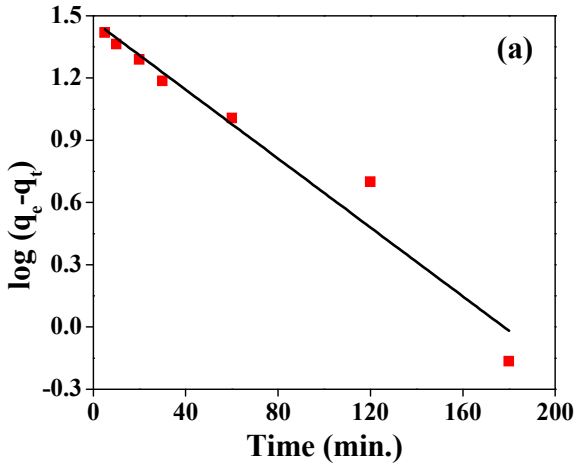

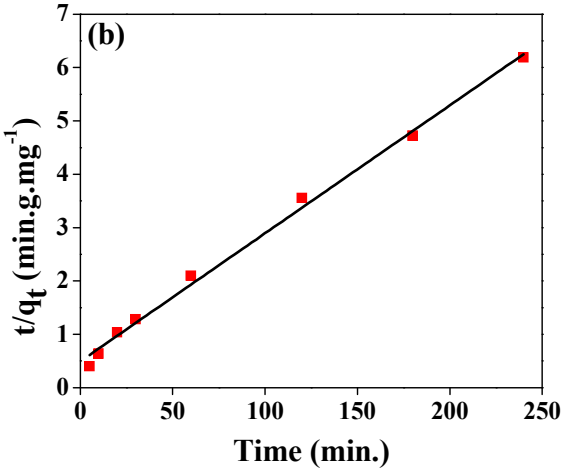

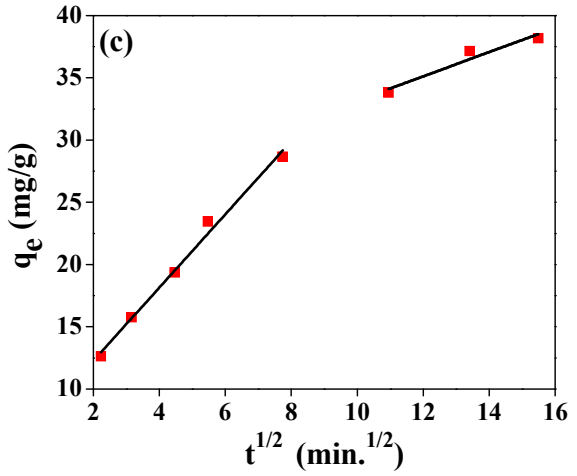

Fig. 11

Table 1

	Adsorbents	q_{max} (mg/g)	pH	T (K)	Ref.
1.	Natural clinoptilolite zeolite	2.88	5	298	55
2.	Nanoporous zirconium oxophosphate	3.3	7.5	295	56
3.	Hematite	5.6	5.5	298	57
4.	Activated carbon	10.47	3	283	58
5.	Nanoporous alumina	11.6	6.8	298	59
6.	Quercetin modified Fe_3O_4	12.3	3.7	298	60
7.	Manganese oxide coated zeolite	17.6	6	293	61
8.	Multi-walled carbon nanotubes	24.9	5	298	62
9.	Magnetite nanoparticles	27	5	300	63
10.	Activated charcoal	28.8	3	293	64
11.	Oxidized multi-walled CNT's	33.32	5	298	65
12.	CMC grafted MWCNT's	39.2	5	293	66
13.	Chitosan grafted MWCNT's	39.2	5	298	67
14.	Poly(acrylamidoxime-co-2-acrylamido-2-methylpropane sulfonic acid hydrogel	39.49	3	298	68
15.	Hydrazine reduced GO	47	4	293	13
16.	Magnetic Fe_3O_4/SiO_2	52	6	298	69
17.	Nanocrystalline titanium dioxide	60	6	293	70
18.	Mesoporous carbon CMK-5	65.4	4	298	71
19.	Fe_3O_4/Graphene oxide composites	69.49	5.5	293	51
20.	Cross-linked chitosan	72.46	3	293	72
21.	Graphene oxide nanosheets	97.5	5	293	40
22.	Poly(methacryllicacid)-grafted chitosan/bentonite composite	117	5.5	298	2
23.	Poly(itaconicacid)-poly(methacrylicacid)-grafted-nanocellulose/nanobentonite composite	119.63	5.5	298	73

24.	GO@sepiolite composites	161.29	4.5	298	74
25.	GO supported chitosan	225.78	4	303	54
26.	Polyaniline modified GO	242.52	3	298	75
27.	3D layered double hydroxide/graphene hybrid material	277.8	4	298	76
28.	Amidoximated magnetite/GO	284.9	5	298	21
29.	GO-activated carbon felt	298	5.5	293	20
30.	NH_3-GO	80.13	6	298	This study